Laboratory Investigation (2019) 99:399–410
https://doi.org/10.1038/s41374-018-0116-6

ARTICLE

The cofilin phosphatase slingshot homolog 1 restrains angiotensin II-induced vascular hypertrophy and fibrosis in vivo

Holly C. Williams[1] · Jing Ma[2,3] · Daiana Weiss[1] · Bernard Lassègue[1] · Roy L. Sutliff[2,3] · Alejandra San Martín[1]

Received: 10 October 2017 / Revised: 30 June 2018 / Accepted: 26 July 2018 / Published online: 5 October 2018

Abstract

The dual specificity phosphatase slingshot homolog 1 (SSH1) contributes to actin remodeling by dephosphorylating and activating the actin-severing protein cofilin. The reorganization of the actin cytoskeleton has been implicated in chronic hypertension and the subsequent mechano-adaptive rearrangement of vessel wall components. Therefore, using a novel $Ssh1^{-/-}$ mouse model, we investigated the potential role of SSH1 in angiotensin II (Ang II)-induced hypertension, and vascular remodeling. We found that loss of SSH1 did not produce overt phenotypic changes and that baseline blood pressures as well as heart rates were comparable between $Ssh1^{+/+}$ and $Ssh1^{-/-}$ mice. Although 14 days of Ang II treatment equally increased systolic blood pressure in both genotypes, histological assessment of aortic samples indicated that medial thickening was exacerbated by the loss of SSH1. Consequently, reverse-transcription quantitative PCR analysis of the transcripts from Ang II-infused animals confirmed increased aortic expression levels of fibronectin, and osteopontin in $Ssh1^{-/-}$ when compared to wild-type mice. Mechanistically, our data suggest that fibrosis in SSH1-deficient mice occurs by a process that involves aberrant responses to Ang II-induced TGFβ1. Taken together, our work indicates that Ang II-dependent fibrotic gene expression and vascular remodeling, but not the Ang II-induced pressor response, are modulated by SSH1-mediated signaling pathways and SSH1 activity is protective against Ang II-induced remodeling in the vasculature.

Hypertension is a pathological state characterized by increased humoral signaling and chronically elevated strain on the cellular components of the arterial wall. One of the consequences of hypertension is the induction of gene expression related to inflammation, fibrosis, and hypertrophy in vascular cells [1–3]. Although inflammation may induce hypertension-related cardiovascular complications, the molecular pathways that result in hypertension-induced inflammation, fibrosis, and hypertrophy are incompletely understood.

During hypertension vascular smooth muscle cells (VSMCs), a main component of the vessel wall, adapt to their altered mechanical and chemical environment by undergoing phenotypic modulation. Specifically, in angiotensin II (Ang II)-induced hypertension, vascular remodeling is associated with increased activity of the transcription factors nuclear factor kappa B (NF-κB) [1, 4, 5], activator protein (AP-1) [6, 7], and CRE-binding protein (CREB) [8, 9] leading to the upregulation of monocyte chemoattractant protein 1 (MCP-1) [2], transforming growth factor β (TGFβ) [10, 11], osteopontin (OPN) [12–14], fibronectin (FN1) [11, 15–17], and collagens (COL) [16, 18] in VSMCs.

The actin cytoskeleton is a dynamic network that regulates several key cellular processes such as contraction, migration, rheology, proliferation, mechanotransduction, and gene expression [19–22]. Importantly, the actin cytoskeleton has also been shown to participate in the cellular responses initiated by Ang II [23, 24] and mechanotransduction [25, 26]. The actin-binding protein cofilin and its upstream activator slingshot phosphatase (SSH1) are key

Supplementary Information The online version of this article (https://doi.org/10.1038/s41374-018-0116-6) contains supplementary material, which is available to authorized users.

✉ Alejandra San Martín
asanmartin@emory.edu

[1] Department of Medicine, Division of Cardiology, Emory University, Atlanta, GA 30322, USA

[2] Atlanta Veterans Affairs Medical Center, Decatur, GA 30033, USA

[3] Division of Pulmonary, Allergy, Critical Care, and Sleep, Department of Medicine, Emory University, Atlanta, GA 30322, USA

regulators of actin dynamics [27–29]. Indeed, our previous work has shown that, in VSMCs, this pathway is required for platelet-derived growth factor (PDGF)-induced migration [30, 31] and adaptation to mechanical strain [25]. Furthermore, in the vasculature SSH1 expression is upregulated during neointima formation [32], dysregulated in a Fbln4$^{-/-}$ model of aortic aneurysm formation [33], and promotes the transition of blood monocytes toward a hypermigratory proatherogenic phenotype [34]. SSH1 has also been implicated in inflammatory signaling via regulation of NF-κB activity in endothelial [35], immune [36], and epithelial cells [37]. Therefore, we hypothesize that SSH1 plays a key role in vascular remodeling during Ang II-induced hypertension.

With the generation of a *Ssh1*$^{-/-}$ mouse model, we demonstrate that loss of SSH1 exacerbates Ang II-induced fibrosis by upregulating the expression of OPN, and FN1 in the aorta. Our data also indicate that SSH1-deficient cells display an abnormal response to TGFβ1 downstream of Ang II-mediated signaling.

Materials and methods

Generation of *Ssh1*$^{-/-}$ mice

Mice with a gene trap inserted into the second intron of the *Ssh1* gene were produced by Taconic Biosciences. Briefly, *Ssh1*$^{-/-}$ mice were generated from an OmniBank clone of embryonic stem cells made by Lexicon Pharmaceuticals [38]. These 129/SvEv stem cells were injected into C57BL/6 albino blastocysts, which were then transferred into the uterus of a host female. Heterozygote founders were produced and backcrossed at least seven generations and wild-type littermates were used as controls. Mice used in the following experiments were 4–6 months of age. Animals were conventionally housed in the Division of Animal Research facilities at Emory University or the Atlanta Veterans Affairs Medical Center and were given regular chow and water ad libitum. All procedures using animals were reviewed and approved by both the Emory University and the Atlanta Veterans Affairs Medical Center Institutional Animal Care and Use Committees and were performed according to National Institutes of Health criteria.

Blood pressure measurement and osmotic minipump implantation

Ssh1$^{+/+}$ and *Ssh1*$^{-/-}$ mice were implanted with telemetry devices to measure baseline blood pressure and heart rate, as previously described [39]. In short, mice were implanted with sterile PA-C10 blood pressure probes (Data Sciences International) and then allowed to fully recover for 7 days prior to the initiation of data collection. Blood pressures were then monitored for 10 s each minute for a 24-h period. Additionally, systolic blood pressure was measured by computer-assisted tail-cuff transmission photoplethysmography, (Visitech Systems) in *Ssh1*$^{+/+}$ and *Ssh1*$^{-/-}$ mice infused with Ang II. To establish baseline blood pressure, mice were habituated to the procedure for 4–5 days and only the last day's measurements are included in the results. Average systolic blood pressure was calculated from the arithmetic mean of ten successive measurements. In experiments involving Ang II-induced hypertension, mice were anesthetized and osmotic minipumps (Azlet) containing [Asn1, Val5]-Ang II (Sigma) (750 μg/kg/day) or 0.9% saline were subcutaneously implanted into the mice, as previously described [40, 41]. Blood pressure was measured over 14 days. Aortas from these animals were later harvested for RNA, protein, or histology.

Vascular contractility and stiffness measurements

Vascular contractility and stiffness was measured as previously described [42, 43]. In short, *Ssh1*$^{+/+}$ and *Ssh1*$^{-/-}$ mice were killed by CO_2 asphyxiation and their aortas were quickly excised and cut into ~5 mm rings. The rings were then mounted on hooks that were attached to a Harvard Apparatus Differential Capacitor Force Transducer and resting tension of each aorta was set at 15 mN. Contractility was assessed by generating concentration response curves to potassium chloride (KCl, 0–80 mM) and phenylephrine (PE, 0.1 nM–10 μM). Data were obtained using Powerlab hardware (AD Instruments) and were analyzed with LabChart software (AD Instruments). Generated forces were expressed as percentages of the maximal force produced in response to KCl or PE. In studies assessing aortic stiffness, rings were mounted between two wires in an organ bath and maximally dilated with 30 μM sodium nitroprusside. The distance between the wires was increased until a deflection in the force measurement was observed. The distance between the two wires was then further increased in 10-μm increments while tension was monitored.

RNA isolation and reverse-transcription qPCR

Whole aortas were harvested from CO_2-killed mice and adherent fat was carefully removed. Aortas were homogenized with a motorized rotor/stator device and RNA was purified from the resulting homogenate using the RNeasy kit (Qiagen). First-strand cDNA synthesis was performed using 1 μg of total RNA, random 15-mer primers, and Superscript II reverse transcriptase (Invitrogen) following the manufacturer's instructions. PCR reactions included Platinum Taq DNA polymerase (Invitrogen) and SYBR Green (Invitrogen). Mouse-specific primers to detect Ssh1 (Qiagen), Ssh2 (Qiagen), TGFβ1 (Qiagen), COL1α1 (Forward—5′-CCTAAGG

GT CCCCAATGGTGAGACG-3′; Reverse—5′-GGGGGTT GGGACAGTCCAGTTCTTC-3′), FN1 (Forward—5′-CTCA ACCTCCCTGAAA CGGCCAACT-3′; Reverse—5′-TCTT GGGGTGCCAGTGGTCTCTTGT-3′), and OPN (Forward —5′-CTTTTGCCTATTTGGCATTGCCTCCTC-3′; Reverse —5′-CACAGAATCCTCGTTCTCTGCATGGT-3′) were used in the subsequent reactions and message expression was quantified using the LightCycler Instrument (Roche Applied Science). Data analysis was performed using the mak3 module of the qpcR software library in the R environment [44, 45].

Western blotting

Mouse aortas were harvested, cleaned of fat and connective tissue, and then flash frozen in liquid nitrogen. Frozen aortas were ground into a fine powder using a pre-chilled mortar and pestle. Proteins were extracted in Hunters buffer (25 mmol/L HEPES, 150 mmol/L KCl, 1.5 mmol/L $MgCl_2$, 1 mmol/L EGTA, 10 mmol/L Na-pyrophosphate, 10 mmol/L NaF, 1% Na deoxycholate, 1% Triton X-100, 0.1% SDS, 10% glycerol, Na-orthovanadate, and protease inhibitors) and lysates were sonicated and then cleared at $10{,}000 \times g$ for 5 min. Proteins were separated using SDS-PAGE and transferred to Immobilon-P polyvinylidene difluoride (PVDF) membranes (Millipore), blocked with 5% non-fat dairy milk, and incubated with primary antibodies to SSH1 (Cell Signaling Cat# 13578), p-cofilin ser-3 (Cell Signaling Cat# 3311), cofilin (Gentex Cat# GTX102156), OPN (R&D# AF808), TGFβ1 (Cell Signaling# 3711), TGFβRII (Santa Cruz Cat# sc-17799) smooth muscle 22 (SM22) (Abcam 14106) or β-actin (Sigma Cat# A5441). Subsequently, blots were incubated with horseradish peroxidase-conjugated secondary antibodies and proteins were detected by enhanced chemiluminescence (ECL, Millipore). Images were acquired using a Carestream Molecular Imaging (Carestream) device. Band intensity was quantified by densitometry using ImageJ software (NIH).

Histology and morphometric assessment

Mice were euthanized using CO_2 and tissues were pressure perfused with saline and fixed with 10% buffered formalin. Whole aortas were excised, paraffin embedded, and cut into 5 µm sections. Aortas were stained with hematoxylin and eosin for morphometric analysis and stained with Masson's Trichrome to evaluate fibrotic regions of the vessel. Images were acquired with the NanoZoomer SQ (Hamamatsu) slide scanner using a ×40 objective and NDP.scan software. Morphometric measurements of the aorta were performed using ImageJ (NIH) and NDP.view2 software (Hamamatsu). Image analysis included aortas from three to six animals per treatment group and three–four sections per aorta.

For immunofluorescent imaging, sections were blocked and then incubated with smooth muscle α2-actin (α-SMA) (Sigma Cat# A5228), calponin 1 (CCN1) (Sigma Cat# 231-R1), or FN1 (Millipore Cat# AB2033) primary antibodies overnight at 4 °C. The sections were washed and incubated with species-specific secondary antibodies conjugated with Alexa Fluor 598 (Jackson Immunoresearch Cat# 711-585-152). Sections treated with secondary antibodies alone did not show specific staining. Confocal micrographs were acquired with a Zeiss LSM 510 META Laser Scanning Confocal Microscope System using a ×20 air objective lens and Zeiss ZEN acquisition software. When comparing sections from different experimental groups, all image threshold settings of the confocal microscope remained constant. Image analysis included aortas from three to five animals per treatment group and three–four sections per aorta. Mean fluorescence intensity and percent area were calculated using ImageJ software (NIH).

Statistics

Results are expressed as means ± SEM. Differences among groups were analyzed using Student's t test and two-way analysis of variance (ANOVA), followed by the Bonferroni post hoc test. A value of $P < 0.05$ was considered statistically significant.

Results

Characterization of C57BL/6J-SSH$^{Gt(OST146683)Lex}$ mice

To examine the contribution of SSH1 to vascular homeostasis and pathology, we generated a global knockout mouse using an embryonic stem cell clone with a gene trap construct inserted into the second intron of the *Ssh1* gene (chromosome 5 NCBI Gene ID: 231637) (Supplemental Fig. 1a). The successful disruption of the target gene was initially confirmed by evaluating mRNA expression in the cerebellum and bladder via reverse-trancription quantitative PCR (RT-qPCR) (data not shown). Lack of SSH1 phosphatase did not result in increased embryonic or perinatal lethality (Supplemental Fig. 1B) and, compared to their littermates, $Ssh1^{-/-}$ mice grow with normal weight gain (Supplemental Fig. 1C) and without obvious abnormalities in their general appearance.

Loss of *Ssh1* mRNA and protein expression in the aorta was verified by quantitative real-time PCR and western blot. *Ssh1* mRNA levels were reduced by ~90% in aortic $Ssh1^{-/-}$ samples when compared to samples from $Ssh1^{+/+}$ (Fig. 1a).

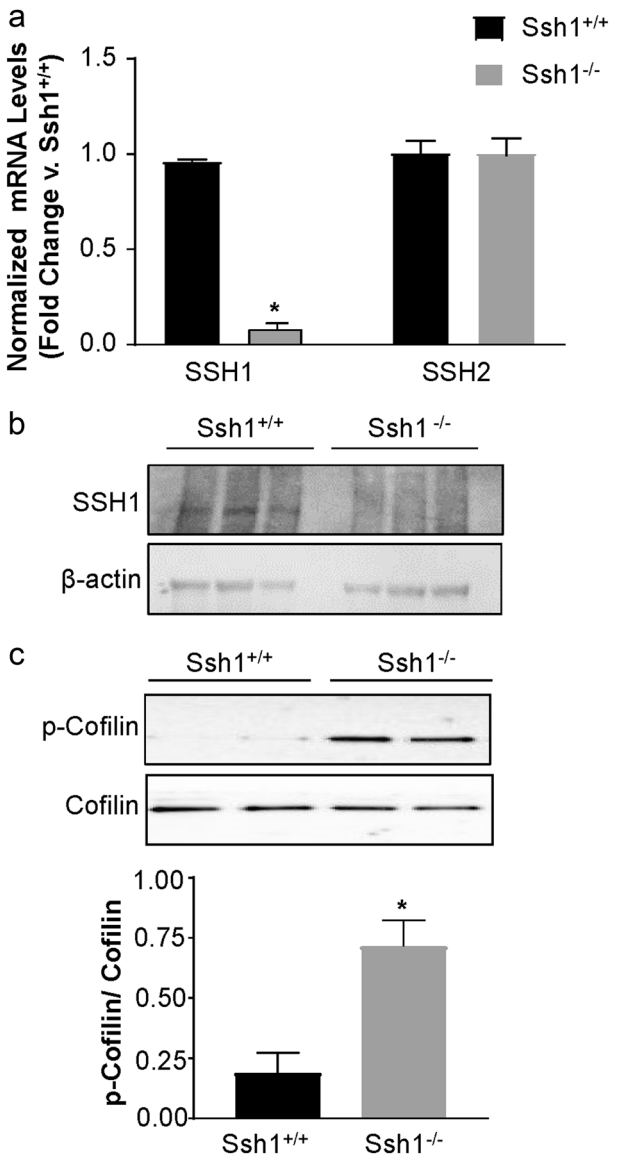

Fig. 1 Confirmation of SSH1 knockout by RT-qPCR and western blot. **a** The aortas of $Ssh1^{+/+}$ and $Ssh1^{-/-}$ mice were harvested for mRNA. SSH1 and SSH2 mRNAs were measured by RT-qPCR and corrected by housekeeping gene PGK. Values are represented as fold change vs. $Ssh1^{+/+}$ ($^*p < 0.0001$, $n = 4$ mice per group). Protein was harvested from the aortas of $Ssh1^{+/+}$ and $Ssh1^{-/-}$ mice, analyzed by western blot and probed with antibodies to **b** SSH1 and actin (representative blot, $n = 2$) or **c** p-Cofilin, and Cofilin. Measurable changes in protein expression were quantified using densiometric analysis ($^*p < 0.006$, $n = 5$–8 mice per group)

Importantly, *Ssh1* deletion did not significantly alter the expression of the known paralog gene *Ssh2* in the aorta (Fig. 1a). At the protein level, SSH1 expression was undetectable in aortic samples harvested from $Ssh1^{-/-}$ mice, while protein samples from $Ssh1^{+/+}$ aortas contained a band that migrated around 130 kDa, which is the predicted molecular weight of SSH1 (Fig. 1b). Using phospho-specific antibodies, we confirmed that aortas from $Ssh1^{-/-}$ mice have significantly more phosphorylated, and therefore inactive cofilin than littermate controls (Fig. 1c). These data are consistent with loss of a cofilin phosphatase activity.

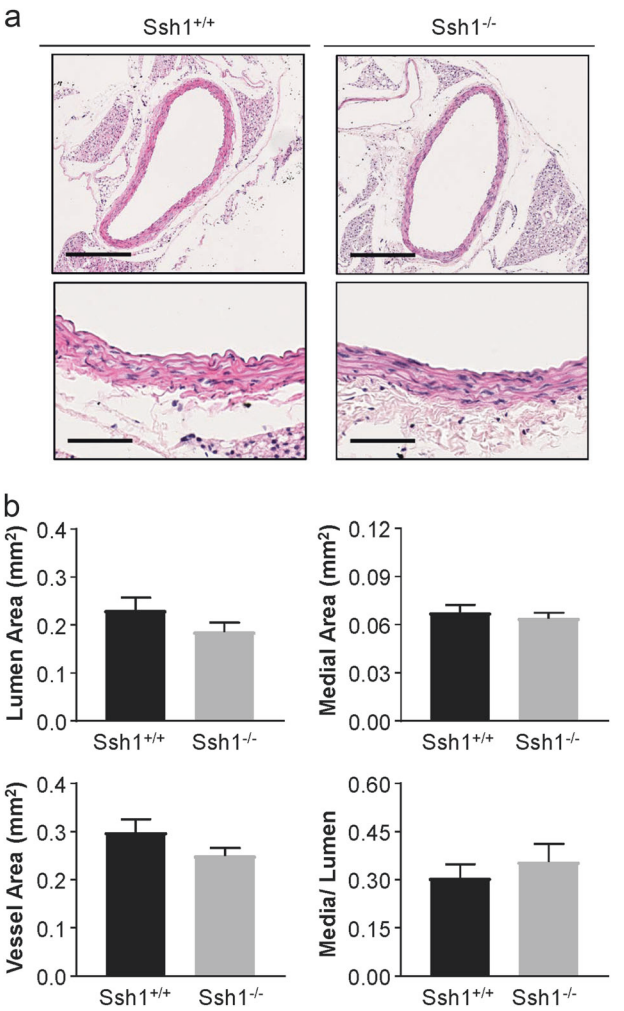

Fig. 2 SSH1 deficiency does not alter aortic structure. **a** The aortas of $Ssh1^{+/+}$ and $Ssh1^{-/-}$ mice were excised, fixed, paraffin embedded, and stained with hematoxylin and eosin. Images were scanned using a ×40 objective (scale bar = 80 μm) as well as ×10 objective (scale bar = 295 μm) images are provided. **b** Lumen area, medial area, total vessel area and, media-to-lumen ratio were calculated after histological evaluation of aortas excised from $Ssh1^{+/+}$ and $Ssh1^{-/-}$ mice

Despite the loss of the phosphatase activity, histological examination of aortas from unchallenged mice did not reveal any overt structural alterations. Morphometric analysis of the hematoxylin and eosin-stained sections indicates that parameters such as lumen area, medial area, total vessel area, and media-to-lumen ratio are equivalent in $Ssh1^{+/+}$ and $Ssh1^{-/-}$ mice (Fig. 2a, b). Additionally, immunofluorescent images of aortic sections show comparable expression of the differentiation markers α-SMA and CNN1 (Supplemental Fig. 2), indicating that VSMC differentiation was unchanged in $Ssh1^{-/-}$ mice in vivo.

Previously, it has been established that during aging intrinsic stiffening of vascular smooth muscle cells is due to

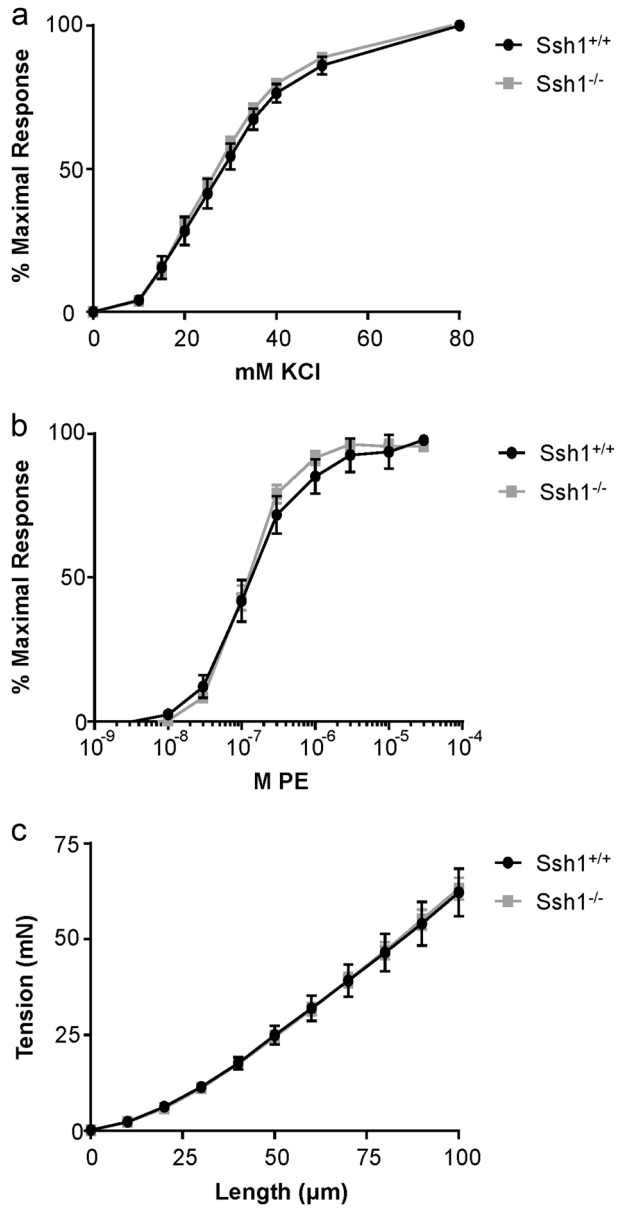

Fig. 3 SSH1 depletion does not affect aortic contractile sensitivity to KCl or PE and aortic stiffness is unaltered by the loss of SSH1. Aortic rings from wild-type and *Ssh1* null mice were isometrically mounted and concentration response curves were generated to **a** KCl and **b** PE. Graphs show the dose–response to KCl and PE normalized to maximum force ($n = 8$–15 mice per group). To evaluate **c** aortic stiffness, aortic segments were incrementally elongated, and the corresponding force was measured ($n = 8$–15 mice per group)

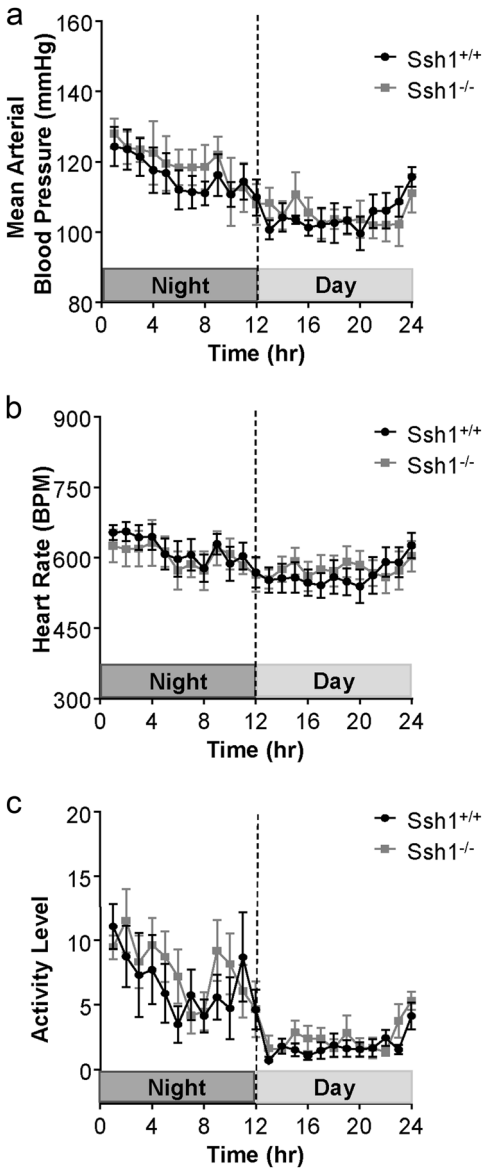

Fig. 4 SSH1 deletion does not significantly alter mean arterial blood pressure, heart rate, or activity levels in mice. $Ssh1^{+/+}$ and $Ssh1^{-/-}$ animals were implanted with telemetry devices and data regarding **a** blood pressure, **b** heart rate, and **c** activity level were recorded over a 24-h period ($n = 4$–6 mice per group)

changes in the actin cytoskeleton and contributes to aortic stiffness [46]. Therefore, we determined if SSH1 deficiency alters the mechanical and contractile properties of the aorta. Isometric forces were measured in isolated aortic rings exposed to increasing concentrations of the α-adrenergic agonist, PE or after depolarization with exogenous KCl. Despite lowered activity of the actin-severing protein cofilin, aortic segments from $Ssh1^{-/-}$ mice did not display significant differences in maximal contraction or force generation in response to KCl (Fig. 3a) or PE (Fig. 3b). Additionally, when aortic segments were incrementally elongated, force generation was also unaltered by loss of the phosphatase (Fig. 3c). These results indicate that the mechanical and contractile properties of the vessels were unchanged by loss of SSH1 expression in basal conditions.

Simultaneously, we used telemetry to evaluate the impact of SSH1 depletion on blood pressure, heart rate, and activity levels. Data from a 24h cycle demonstrates that loss of phosphatase does not significantly alter the mean arterial pressure (Fig. 4a), heart rate (Fig. 4b), or activity levels

Table 1 Chronic angiotensin II infusion increases systolic blood pressure in both Ssh1$^{+/+}$ and Ssh1$^{-/-}$ mice

	N	Systolic blood pressure	Diastolic blood pressure	Mean arterial pressure
Ssh$^{+/+}$				
D0	20	100.3 ± 1.81	74.1 ± 2.63	80.4 ± 2.74
D7	13	147.8 ± 4.48 *	124.8 ± 5.48 *	133.2 ± 5.2 *
D14	7	157.3 ± 3.3 **	126.9 ± 5.89 **	136.5 ± 5.88 **
Ssh1$^{-/-}$				
D0	18	106 ± 3.16	79.8 ± 2.32	88.5 ± 2.6
D7	14	160.6 ± 4.24 #	128.8 ± 5.81 #	139.7 ± 5.07 #
D14	7	160.6 ± 6.186 ##	133.4 ± 8.41 ##	143.4 ± 8.44 ##

Mice were implanted with osmotic minipumps containing Ang II (750 ng/kg/day) or saline. Blood pressure was measured by tail-cuff plethysmography over the course of 14 days (*Ssh1*$^{+/+}$ D0 vs. D7, *$p <$ 0.001, $n = 13$–20 mice per group; *Ssh1*$^{+/+}$ D0 vs. D14, **$p < 0.001$, $n = 7$–20 mice per group; *Ssh1*$^{-/-}$ D0 vs. D7, $^{\#}p < 0.001$, $n = 14$–18 mice per group; *Ssh1*$^{-/-}$ D0 vs. D14, $^{\#\#}p < 0.001$, $n = 7$–18 mice per group)

(Fig. 4c). Taken together, our data indicate that the depletion of SSH1 phosphatase and the concomitant decrease in cofilin activity do not alter aortic architecture, blood pressure, or heart rate in this unchallenged mouse model.

SSH1 depletion does not alter angiotensin II-induced hypertension

Since cytoskeletal reorganization has been implicated in hypertension and vascular inflammation [19, 23, 24], and SSH1 phosphatase regulates stimulus-dependent actin remodeling along with inflammatory signaling in vitro [25, 30, 31, 35, 36], we decided to evaluate the impact of SSH1 depletion on Ang II-induced hypertension and vascular remodeling. First, we examined the consequences of SSH1 depletion on Ang II-induced hypertension using computer-assisted tail-cuff transmission photoplethysmography. Blood pressure was measured at 0, 7, and 14 days post implantation of Ang II or saline-filled osmotic minipumps. After 7 and 14 days of Ang II treatment, we observed significant increases in systolic, diastolic, and mean arterial pressure in both groups of animals (Table 1). Additionally, at 7 days of Ang II systolic blood pressure was slightly elevated in *Ssh1*$^{-/-}$ mice when compared with wild-type controls; however, mean arterial pressure and diastolic blood pressure were comparable between both genotypes (Table 1).

Angiotensin II-induced vascular remodeling and fibrosis are increased in SSH1-deficient mice

Dynamic regulation of the actin cytoskeleton plays a key role in vascular remodeling in response to hypertension

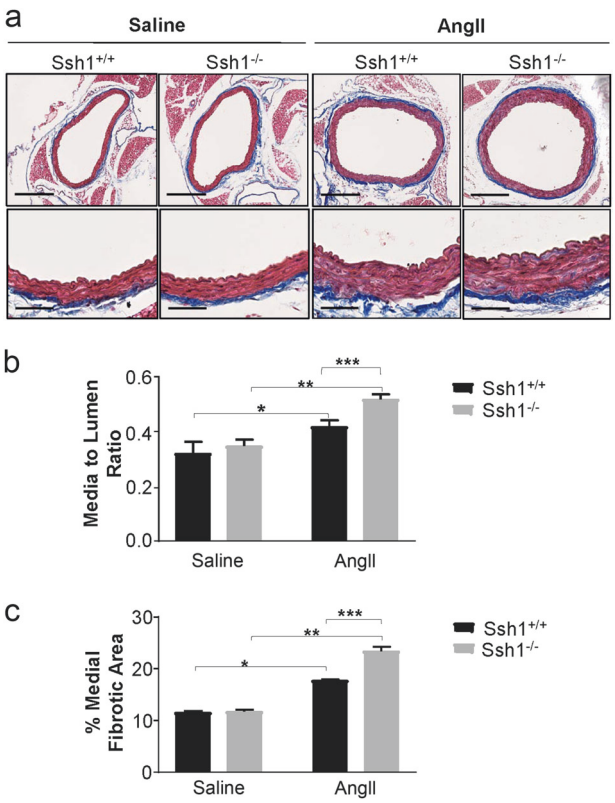

Fig. 5 Loss of SSH1 exacerbates angiotensin II-induced increases in aortic wall thickness and fibrotic matrix deposition. Mice were treated with Ang II or saline for 14 days. Aortas were harvested, embedded in paraffin, cut into 5 µm sections, and stained with Masson's Trichrome. **a** Images were scanned using a ×40 objective (scale bar = 80 µm) as well as a ×10 objective (scale bar = 295 µm). Ang II media changes in aortic structure were evaluated by measuring changes in the **b** media-to-lumen ratio of *Ssh1*$^{+/+}$ and *Ssh1*$^{-/-}$ mice using ImageJ software. (*$p = 0.04$, $n = 3$–5; **$p < 0.001$, $n = 3$–6 mice per group; ***$p < 0.001$, $n = 3$–6 mice per group). **c** Medial fibrotic matrix deposition (*$p < 0.001$, $n = 3$–4; **$p < 0.001$, $n = 3$–5 mouse per group; ***$p < 0.001$, $n = 3$–5 mice per group) was quantified by ImageJ

[47, 48]. Thus, we examined if there were changes in the aortic structure and composition between *Ssh1*$^{+/+}$ and *Ssh1*$^{-/-}$ animals after 14 days of Ang II treatment. Aortic sections were stained for morphometric analysis and fibrosis within the vascular wall with hematoxylin and eosin (Supplemental Fig. 3) or Masson's Trichrome (Fig. 5a), respectively. Predictably, Ang II treatment increased the media-to-lumen ratio in both genotypes when compared to saline controls (Fig. 5b). Interestingly, the Ang II-mediated changes in media-to-lumen ratio were further increased in *Ssh1*$^{-/-}$ mice (Fig. 5b). Ang II treatment also significantly increased the percentage of medial fibrotic staining when compared to saline in both groups (Fig. 5c). In agreement with the increase in aortic hypertrophy, medial fibrosis was also exacerbated by the loss of SSH1 (Fig. 5c).

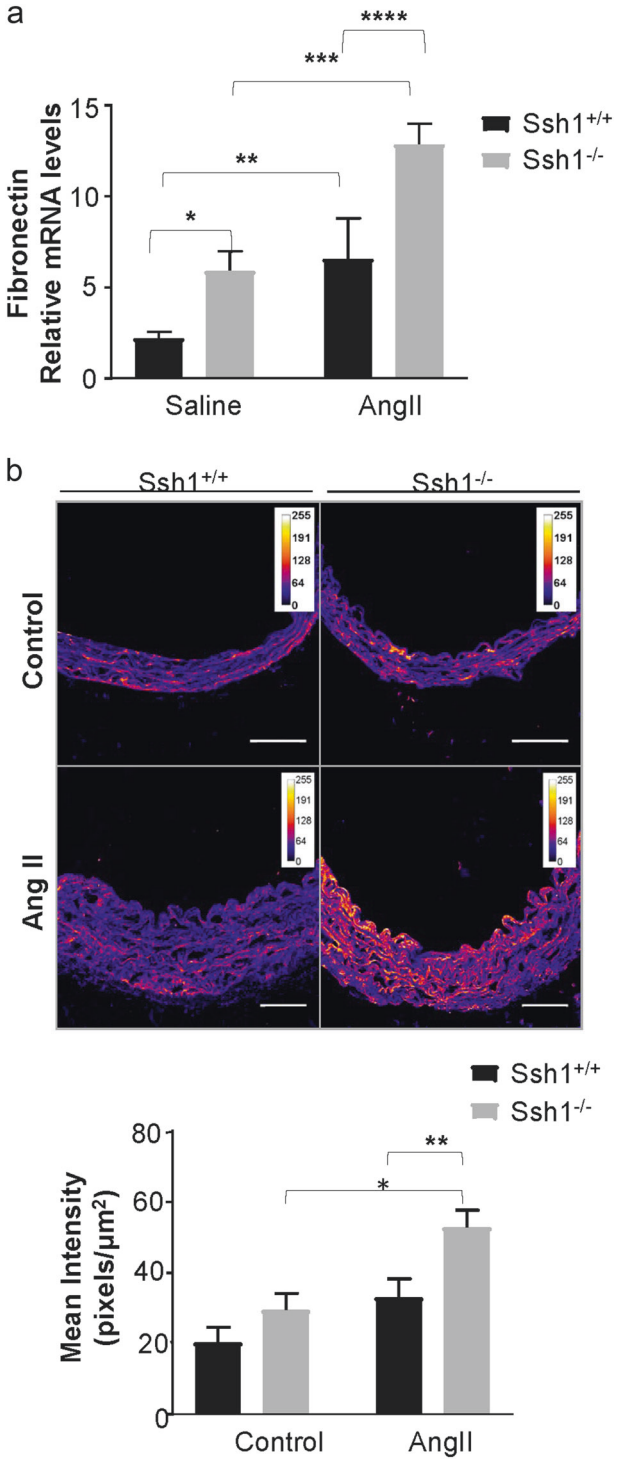

◀ **Fig. 6** SSH1 depletion potentiates aortic fibronectin expression. *Ssh1*$^{+/+}$ and *Ssh1*$^{-/-}$ mice were implanted with osmotic minipumps containing Ang II or saline for 10 days. Aortas from these mice were harvested for mRNA and **a** *Fn1* expression was evaluated by RT-qPCR (*$p = 0.0009$, $n = 4$–10 mice per group; **$p = 0.0437$, $n = 8$–10 mice per group; ***$p = 0.0183$, $n = 4$–6 mice per group; ****$p = 0.0120$, $n = 6$–8 mice per group). Aortic sections from *Ssh1*$^{+/+}$ and *Ssh1*$^{-/-}$ mice treated with Ang II for 14 days were stained with a FN1 antibody. **b** Confocal images were acquired using a ×20 air objective lens (scale bar = 70 μm) and immunofluorescent staining was quantified using ImageJ software. (*$p = 0.0132$, $n = 3$–6 mice per group; **$p = 0.0208$, $n = 4$–6 mice per group)

Angiotensin II induces expression of SSH1 phosphatase and loss of SSH1 potentiates vascular fibrotic gene expression

Consistent with an increase in vascular fibrosis after Ang II treatment, aortas from *Ssh1*$^{-/-}$ mice displayed marked increases in *Fn1* mRNA expression (Fig. 6a) and protein deposition (Fig. 6b) when compared to wild-type mice. Additionally, Ang II-induced OPN mRNA and protein levels were exacerbated in the aortas of mice deficient in SSH1 (Fig. 7a–c). Interestingly and in agreement with the idea that its expression limits vascular fibrosis, *Ssh1* mRNA expression was considerably increased in wild-type animals after Ang II treatment (Supplemental Fig. 4). In contrast, Ang II-induced *ColIa1* mRNA and protein deposition were comparable between genotypes (Fig. 8a, b). Consistent with the fact that collagen I expression is a major contributor to aortic stiffness [49], the mechanical properties of the SSH1-deficient aortas were unchanged in the 2-week experimental period when compared to wild-type animals (Supplemental Fig. 5).

SSH1 deficiency amplifies TGFβ1-induced fibrotic gene expression

The fact that *Ssh1*$^{-/-}$ mice preserve vascular integrity and their arteries have similar mechanical properties than wild-type animals suggested to us that SSH1 deficiency is unlikely to affect the strain within the vessel wall and that the exacerbation of Ang II-induced fibrotic gene expression may be the consequence of an intrinsic differential response to Ang II-initiated signaling.

The fibrotic response observed in the aortas of *Ssh1*$^{-/-}$ animals resembles the activation of the TGFβ pathway. Indeed, the increase in circulating Ang II levels induced the expression of TGFβ1 mRNA (Fig. 9a) and protein levels (Fig. 9b). However, this response was not different between wild-type and SSH1-deficient animals. Additionally, TGFβR2 protein levels did not significantly differ between the two genotypes. These data indicated that SSH1 deficiency affected the signaling pathway downstream of TGFβ1. In order to test this hypothesis and gain insight into the mechanism by which SSH1 deficiency exacerbates aortic fibrosis, we used 13 dpc embryos to prepare mouse embryonic fibroblasts (MEFs) and performed in vitro experiments.

After confirmed loss of SSH1 (Supplemental Fig. 6A) expression and increase in the phosphorylated (inactive) form of its substrate cofilin (Supplemental Fig. 6B), cells were

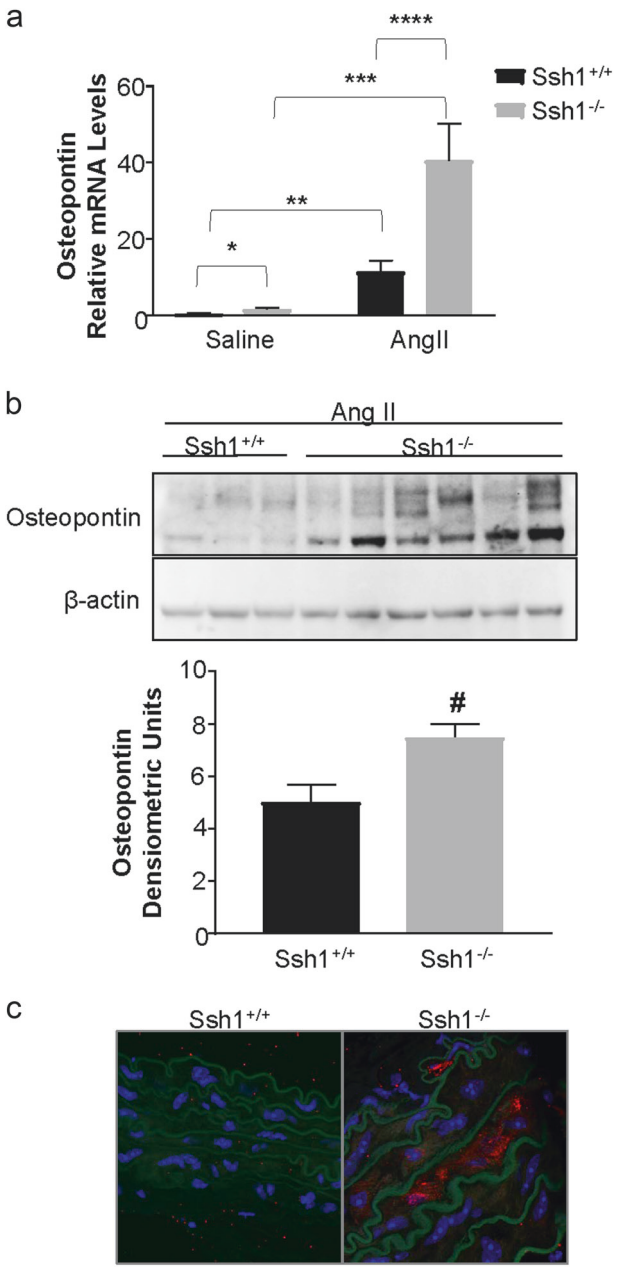

Fig. 7 Loss of SSH1 exacerbates angiotensin II-induced aortic osteopontin expression. *Ssh1*$^{+/+}$ and *Ssh1*$^{-/-}$ mice were implanted with osmotic minipumps containing Ang II or saline for 10 days. Aortas were harvested for mRNA and **a** *Opn* expression was evaluated by RT-qPCR (*$p = 0.0038$, $n = 7$–9 mice per group; **$p = 0.0074$, $n = 5$–9 mice per group; ***$p < 0.0001$, $n = 3$–7 mice per group; ****$p < 0.0001$, $n = 3$–5 mice per group). Protein was harvested from the aortas of *Ssh1*$^{+/+}$ and *Ssh1*$^{-/-}$ mice treated with Ang II, analyzed by western blot and probed with antibodies to **b** OPN. Band intensity was measured using ImageJ ($^{\#}p = 0.0206$, $n = 3$–6 mice per group). Aortic sections from *Ssh1*$^{+/+}$ and *Ssh1*$^{-/-}$ mice treated with Ang II were stained with an OPN antibody. **c** Confocal images were acquired using a ×63 oil objective lens (scale bar = 20 μm) (representative micrographs, $n = 3$ mice per group)

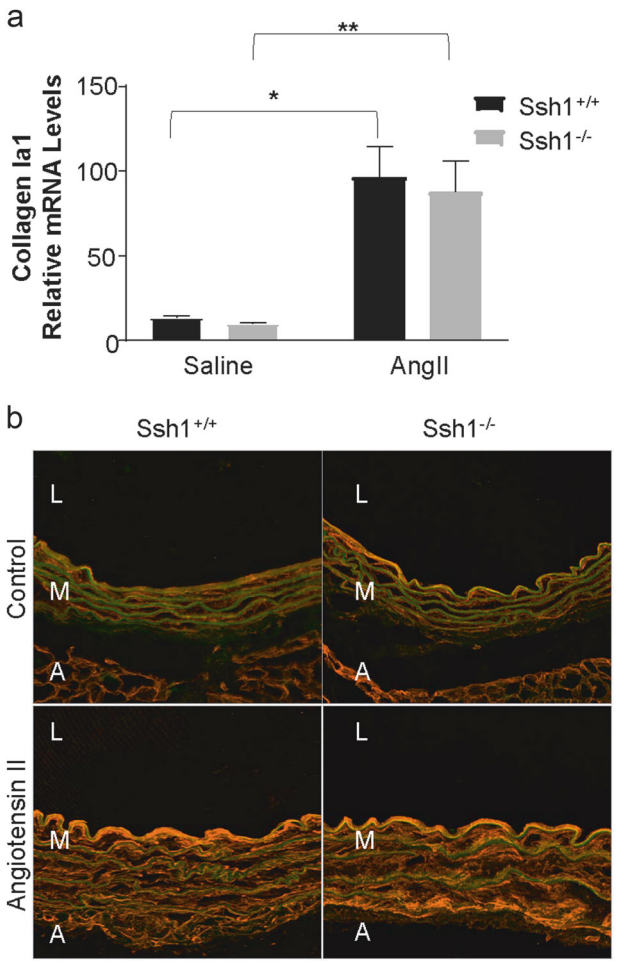

Fig. 8 *Ssh1* deletion does not alter angiotensin II-mediated collagen I expression in the aorta. Ssh1$^{+/+}$ and Ssh1$^{-/-}$ mice were implanted with osmotic minipumps containing Ang II or saline for 10 days. mRNA was harvested from each aorta and **a** *ColIa1* expression was evaluated by RT-qPCR (*$p < 0.0001$, $n = 6$–10 mice per group; **$p = 0.0011$, $n = 4$–6 mice per group). Aortic sections from Ssh1$^{+/+}$ and Ssh1$^{-/-}$ mice treated with Ang II for 14 days were stained with a **b** collagen I antibody and confocal images were acquired using a 20x air objective lens (scale bar = 100 μm) (representative micrographs, $n = 3$–5 mice per group)

exposed to TGFβ1. We confirmed that MEFs from *Ssh1*$^{+/+}$ and *Ssh1*$^{-/-}$ mice expressed comparable levels of TGFβR2 (Supplemental Fig. 6C), but SSH1-deficient cells produced significantly higher amount of OPN when compared to wild-type cells (Fig. 10a). Interestingly, this exacerbated response to TGFβ1 does not encompass contractile proteins (Fig. 10b) and seems to be specific to fibrotic responses. This result demonstrates that SSH1 deficiency increases TGFβ1 signaling and suggests that vascular fibrosis is the result of exacerbated response to TGFβ1 in *Ssh1*$^{-/-}$ mice.

Discussion

Hypertension is characterized in part by humoral factors and chronically elevated strain on the cellular components of the arterial wall. These factors induce pathogenic vascular

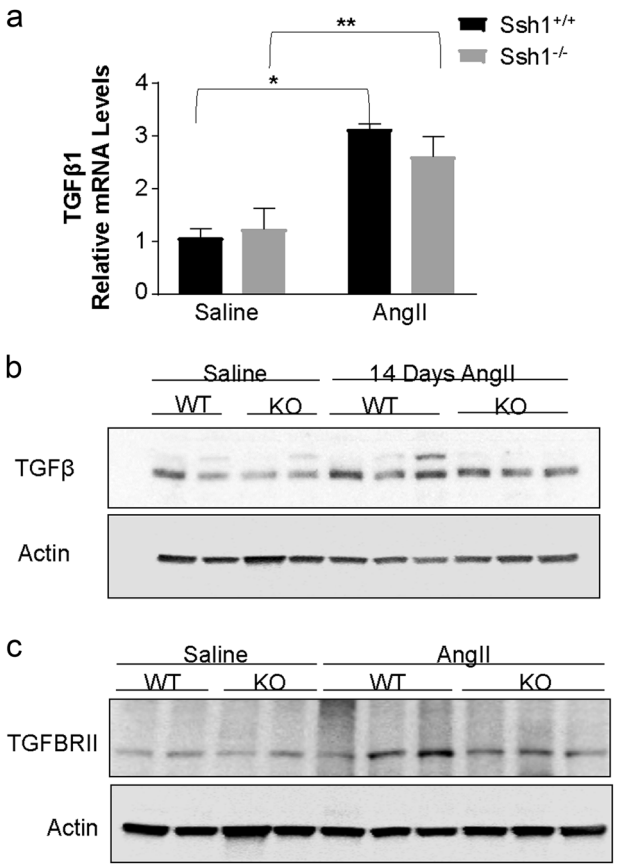

Fig. 9 Angiotensin II induces aortic TGFβ in both $Ssh1^{+/+}$ and $Ssh1^{-/-}$ mice. $Ssh1^{+/+}$ and $Ssh1^{-/-}$ mice were implanted with osmotic minipumps containing Ang II or saline for 10 days. The aortas from these mice were harvested for mRNA and **a** *TGFβ1* expression was evaluated by RT-qPCR ($*p < 0.0001$, $n = 5$–6 mice per group; $**p = 0.0087$, $n = 3$ mice per group). Additionally, protein was harvested from the aortas of $Ssh1^{+/+}$ and $Ssh1^{-/-}$ mice treated with Ang II, analyzed by western blot and probed with antibodies to **b** TGFβ (representative blot, $n = 2$–3 animals per group) and **c** TGFβRII (representative blot, $n = 2$–3 animals per group)

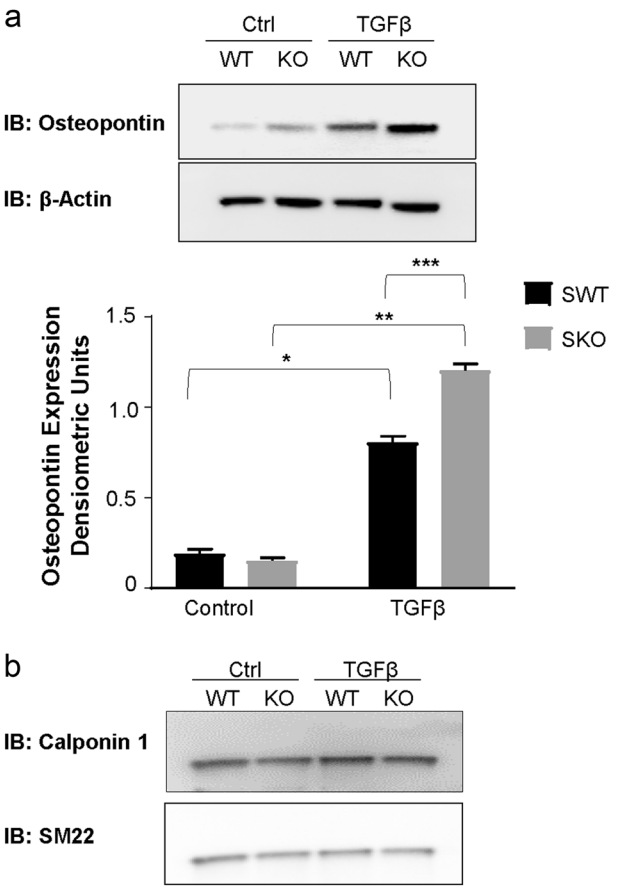

Fig. 10 TGFβ-induced osteopontin expression is exacerbated in $Ssh1^{-/-}$ mouse embryonic fibroblasts. Mouse embryonic fibroblasts were generated from $Ssh1^{+/+}$ and $Ssh1^{-/-}$ embryos and treated with 2 ng/mL TGFβ for 24 h. $Ssh1^{+/+}$ and $Ssh1^{-/-}$ MEFs were harvested for protein and lysates were analyzed by SDS-PAGE and western blot. Membranes were immunoblotted for **a** OPN ($*p < 0.0001$, $n = 6$ independent experiments; $**p < 0.0001$, $n = 6$ independent experiments; $***p < 0.0001$, $n = 6$ independent experiments) **b** CNN1 and SM22 (representative blot, $n = 3$ independent experiments)

remodeling in which the actin cytoskeleton of vascular smooth muscle cells is thought to play a role [47, 48, 50, 51]. Specifically, we investigated the contribution of the actin cytoskeleton-regulating protein, SSH1 to the progression of Ang II-induced hypertension and vascular remodeling. Here, using a unique mouse model deficient in SSH1, we provide the first report about the role of this phosphatase in fibrotic vascular disease. Basally, SSH1 depletion increased aortic cofilin phosphorylation and inactivation. The loss of SSH1 and cofilin activity corresponded with an increase in basal *Opn* and *Fn1* mRNA expression in the aorta. However, these subtle baseline changes caused no overt phenotypic changes in the animal and vascular structure as well as blood pressure were largely unaltered by depletion of the phosphatase.

Under pathophysiological conditions, the Ang II pressor response did not significantly differ between wild-type and knockout animals; however, SSH1 deletion potentiated Ang II-induced fibrotic gene expression. Specifically, loss of SSH1 increased Ang II-dependent fibrotic matrix deposition as measured by Masson's Trichrome stain, in the medial layer of the aorta. These changes were linked to increased Ang II-induced transcription of *Fn1* and *Opn*. Interestingly, we also observed an increase in SSH1 expression in response to Ang II infusion, suggesting that the low basal expression and activity of the phosphatase may explain the absence of a basal vascular phenotype induced by the loss of *Ssh1* gene. Additionally, these data support the idea that SSH1 upregulation may restrain further induction of fibrotic genes in the wild-type animals.

Previous work from our group has established that SSH1 activation occurs downstream of ROS produced by NADPH oxidases [25, 30, 31]. Furthermore, Nox1-based NADPH

oxidase-derived ROS participates in Ang II-induced signaling and intimal hyperplasia in vivo [52]. In agreement with these reports, in our study Ang II treatment induced the expression SSH1 in wild-type animals. Since SSH1 expression restrains vascular hyperplasia, it is possible that Ang II-induced ROS participate in both pro- and anti-fibrotic signaling pathways. Strategies designed to specifically increase SSH1 activity may have a protective role in the pathological vascular remodeling.

The stiffness of the vasculature has been linked with increased collagen deposition over time [49]. Though in our study fibrosis of the vessel wall was exacerbated, we did not observe increased collagen deposition in the SSH1-deficient animals within the designated study period which may explain the preservation of the mechanical properties of the vessels.

The blood vessel wall is exposed to radial, axial, and circumferential strain generated by pulse pressure as blood flows from the heart. Under normal conditions, VSMCs respond to this mechanical strain, by orienting themselves toward the direction of minimal biological perturbation by dramatically reorganizing their cytoskeleton [25, 53–55]. However, in the presence of excessive hemodynamic forces as seen in systemic hypertension the mechanical stress is great and VSMCs switch their phenotype from contractile to synthetic [56–59]. This switch is associated with increased proliferation and production of extracellular matrix proteins [60, 61]. Interestingly, the multifunctional protein OPN and the extracellular matrix protein FN1 are induced in vascular smooth muscle cells in response to stretch and Ang II stimulation [12, 13, 60, 62–65]. Here we demonstrate that *Ssh1*$^{-/-}$ mice have increased OPN and FN1 mRNA expression basally when compared to wild-type littermates and that the loss of SSH1 further potentiates the Ang II-dependent increase in aortic OPN and FN1 mRNA. Importantly, the increases in Ang II-mediated OPN and FN1 occur without overt changes in blood pressure between the wild-type and knockout groups. This observation suggests that SSH1 may play a role in transducing mechanical forces into chemical signals. Specifically, we found that SSH1 modulates TGFβ1 signaling. Interestingly, this modulation seems specific to certain fibrotic proteins and did not extend to the regulation of differentiation markers such as CNN1 or SM22.

Based on our current and previous findings, we propose that the actin regulator SSH1 normally acts to block fibrotic gene expression in response to the increased mechanical and humoral stress imposed by Ang II-induced hypertension.

Acknowledgements This study was supported by The National Heart, Lung and Blood Institute of the National Institutes of Health under awards HL095070 and HL113167. Microscopy experiments were performed in the Microscopy in Medicine Core, supported by NIH grant P01 HL095070.

Compliance with ethical standards

Conflict of interest The authors declare that they have no conflict of interest.

References

1. Sanz-Rosa D, Oubina MP, Cediel E, de Las Heras N, Vegazo O, Jimenez J, et al. Effect of AT1 receptor antagonism on vascular and circulating inflammatory mediators in SHR: role of NF-kappaB/IkappaB system. Am J Physiol Heart Circ Physiol. 2005;288:H111–5.
2. Capers Qt, Alexander RW, Lou P, De Leon H, Wilcox JN, Ishizaka N, et al. Monocyte chemoattractant protein-1 expression in aortic tissues of hypertensive rats. Hypertension. 1997;30:1397–402.
3. Luvara G, Pueyo ME, Philippe M, Mandet C, Savoie F, Henrion D, et al. Chronic blockade of NO synthase activity induces a proinflammatory phenotype in the arterial wall: prevention by angiotensin II antagonism. Arterioscler Thromb Vasc Biol. 1998;18:1408–16.
4. Zahradka P, Werner JP, Buhay S, Litchie B, Helwer G, Thomas S. NF-kappaB activation is essential for angiotensin II-dependent proliferation and migration of vascular smooth muscle cells. J Mol Cell Cardiol. 2002;34:1609–21.
5. Muller DN, Dechend R, Mervaala EM, Park JK, Schmidt F, Fiebeler A, et al. NF-kappaB inhibition ameliorates angiotensin II-induced inflammatory damage in rats. Hypertension. 2000;35(1 Pt 2):193–201.
6. Morishita R, Gibbons GH, Horiuchi M, Kaneda Y, Ogihara T, Dzau VJ. Role of AP-1 complex in angiotensin II-mediated transforming growth factor-beta expression and growth of smooth muscle cells: using decoy approach against AP-1 binding site. Biochem Biophys Res Commun. 1998;243:361–7.
7. Yoshizumi M, Tsuchiya K, Suzaki Y, Kirima K, Kyaw M, Moon JH, et al. Quercetin glucuronide prevents VSMC hypertrophy by angiotensin II via the inhibition of JNK and AP-1 signaling pathway. Biochem Biophys Res Commun. 2002;293:1458–65.
8. Yang J, Jiang H, Chen SS, Chen J, Xu SK, Li WQ, et al. CBP knockdown inhibits angiotensin II-induced vascular smooth muscle cells proliferation through downregulating NF-kB transcriptional activity. Mol Cell Biochem. 2010;340:55–62.
9. Molnar P, Perrault R, Louis S, Zahradka P. The cyclic AMP response element-binding protein (CREB) mediates smooth muscle cell proliferation in response to angiotensin II. J Cell Commun Signal. 2014;8:29–37.
10. Kim S, Ohta K, Hamaguchi A, Omura T, Yukimura T, Miura K, et al. Angiotensin II type I receptor antagonist inhibits the gene expression of transforming growth factor-beta 1 and extracellular matrix in cardiac and vascular tissues of hypertensive rats. J Pharmacol Exp Ther. 1995;273:509–15.
11. Moriguchi Y, Matsubara H, Mori Y, Murasawa S, Masaki H, Maruyama K, et al. Angiotensin II-induced transactivation of epidermal growth factor receptor regulates fibronectin and transforming growth factor-beta synthesis via transcriptional and posttranscriptional mechanisms. Circ Res. 1999;84:1073–84.
12. Remus EW, Lyle AN, Weiss D, Landazuri N, Weber M, Searles C, et al. miR181a protects against angiotensin II-induced

osteopontin expression in vascular smooth muscle cells. Atherosclerosis. 2013;228:168–74.
13. Caesar C, Lyle AN, Joseph G, Weiss D, Alameddine FMF, Lassègue B. et al. Cyclic strain and hypertension increase osteopontin expression in the aorta. Cell Mol Bioeng. 2017;10:144–52.
14. Dab H, Hachani R, Sakly M, Bricca G, Kacem K. Physiological regulation of pro-inflammatory cytokines expression in rat cardiovascular tissues by sympathetic nervous system and angiotensin II. Gen Physiol Biophys. 2013;32:569–75.
15. Saouaf R, Takasaki I, Eastman E, Chobanian AV, Brecher P. Fibronectin biosynthesis in the rat aorta in vitro. Changes due to experimental hypertension. J Clin Invest. 1991;88:1182–9.
16. Ohta K, Kim S, Hamaguchi A, Yukimura T, Miura K, Takaori K, et al. Role of angiotensin II in extracellular matrix and transforming growth factor-beta 1 expression in hypertensive rats. Eur J Pharmacol. 1994;269:115–9.
17. Nahman NS Jr, Rothe KL, Falkenhain ME, Frazer KM, Dacio LE, Madia JD, et al. Angiotensin II induction of fibronectin biosynthesis in cultured human mesangial cells: association with CREB transcription factor activation. J Lab Clin Med. 1996;127:599–611.
18. Kato H, Suzuki H, Tajima S, Ogata Y, Tominaga T, Sato A, et al. Angiotensin II stimulates collagen synthesis in cultured vascular smooth muscle cells. J Hypertens. 1991;9:17–22.
19. Brozovich FV, Nicholson CJ, Degen CV, Gao YZ, Aggarwal M, Morgan KG. Mechanisms of vascular smooth muscle contraction and the basis for pharmacologic treatment of smooth muscle disorders. Pharmacol Rev. 2016;68:476–532.
20. Vedula P, Kashina A. The makings of the 'actin code': regulation of actin's biological function at the amino acid and nucleotide level. J Cell Sci. 2018;131:jcs215509.
21. Misu S, Takebayashi M, Miyamoto K. Nuclear actin in development and transcriptional reprogramming. Front Genet. 2017;8:27.
22. Xu Q, Huff LP, Fujii M, Griendling KK. Redox regulation of the actin cytoskeleton and its role in the vascular system. Free Radic Biol Med. 2017;109:84–107.
23. Touyz RM, Yao G, Schiffrin EL. Role of the actin cytoskeleton in angiotensin II signaling in human vascular smooth muscle cells. Can J Physiol Pharmacol. 2005;83:91–7.
24. Wesselman JP, De Mey JG. Angiotensin and cytoskeletal proteins: role in vascular remodeling. Curr Hypertens Rep. 2002;4:63–70.
25. Montenegro MF, Valdivia A, Smolensky A, Verma K, Taylor WR, San Martin A. Nox4-dependent activation of cofilin mediates VSMC reorientation in response to cyclic stretching. Free Radic Biol Med. 2015;85:288–94.
26. Ciobanasu C, Faivre B, Le Clainche C. Integrating actin dynamics, mechanotransduction and integrin activation: the multiple functions of actin binding proteins in focal adhesions. Eur J Cell Biol. 2013;92:339–48.
27. Nishita M, Tomizawa C, Yamamoto M, Horita Y, Ohashi K, Mizuno K. Spatial and temporal regulation of cofilin activity by LIM kinase and Slingshot is critical for directional cell migration. J Cell Biol. 2005;171:349–59.
28. Endo M, Ohashi K, Sasaki Y, Goshima Y, Niwa R, Uemura T, et al. Control of growth cone motility and morphology by LIM kinase and Slingshot via phosphorylation and dephosphorylation of cofilin. J Neurosci. 2003;23:2527–37.
29. Huang TY, DerMardirossian C, Bokoch GM. Cofilin phosphatases and regulation of actin dynamics. Curr Opin Cell Biol. 2006;18:26–31.
30. San Martin A, Lee MY, Williams HC, Mizuno K, Lassegue B, Griendling KK. Dual regulation of cofilin activity by LIM kinase and Slingshot-1L phosphatase controls platelet-derived growth factor-induced migration of human aortic smooth muscle cells. Circ Res. 2008;102:432–8.
31. Maheswaranathan M, Gole HK, Fernandez I, Lassegue B, Griendling KK, San Martin A. Platelet-derived growth factor (PDGF) regulates Slingshot phosphatase activity via Nox1-dependent auto-dephosphorylation of serine 834 in vascular smooth muscle cells. J Biol Chem. 2011;286:35430–7.
32. Torres RA, Drake DA, Solodushko V, Jadhav R, Smith E, Rocic P, et al. Slingshot isoform-specific regulation of cofilin-mediated vascular smooth muscle cell migration and neointima formation. Arterioscler Thromb Vasc Biol. 2011;31:2424–31.
33. Yamashiro Y, Papke CL, Kim J, Ringuette LJ, Zhang QJ, Liu ZP, et al. Abnormal mechanosensing and cofilin activation promote the progression of ascending aortic aneurysms in mice. Sci Signal. 2015;8:ra105.
34. Kim HS, Ullevig SL, Nguyen HN, Vanegas D, Asmis R. Redox regulation of 14-3-3zeta controls monocyte migration. Arterioscler Thromb Vasc Biol. 2014;34:1514–21.
35. Leonard A, Marando C, Rahman A, Fazal F. Thrombin selectively engages LIM kinase 1 and slingshot-1L phosphatase to regulate NF-kappaB activation and endothelial cell inflammation. Am J Physiol Lung Cell Mol Physiol. 2013;305:L651–64.
36. Bielig H, Lautz K, Braun PR, Menning M, Machuy N, Brugmann C, et al. The cofilin phosphatase slingshot homolog 1 (SSH1) links NOD1 signaling to actin remodeling. PLoS Pathog. 2014;10:e1004351.
37. Wang QZ, Gao HQ, Liang Y, Zhang J, Wang J, Qiu J. Cofilin1 is involved in hypertension-induced renal damage via the regulation of NF-kappaB in renal tubular epithelial cells. J Transl Med. 2015;13:323.
38. Zambrowicz BP, Friedrich GA, Buxton EC, Lilleberg SL, Person C, Sands AT. Disruption and sequence identification of 2,000 genes in mouse embryonic stem cells. Nature. 1998;392:608–11.
39. Kleinhenz JM, Murphy TC, Pokutta-Paskaleva AP, Gleason RL, Lyle AN, Taylor WR, et al. Smooth muscle-targeted overexpression of peroxisome proliferator activated receptor-gamma disrupts vascular wall structure and function. PLoS ONE. 2015;10:e0139756.
40. Dikalova A, Clempus R, Lassegue B, Cheng G, McCoy J, Dikalov S, et al. Nox1 overexpression potentiates angiotensin II-induced hypertension and vascular smooth muscle hypertrophy in transgenic mice. Circulation. 2005;112:2668–76.
41. Weiss D, Kools JJ, Taylor WR. Angiotensin II-induced hypertension accelerates the development of atherosclerosis in apoE-deficient mice. Circulation. 2001;103:448–54.
42. Sutliff RL, Dikalov S, Weiss D, Parker J, Raidel S, Racine AK, et al. Nucleoside reverse transcriptase inhibitors impair endothelium-dependent relaxation by increasing superoxide. Am J Physiol Heart Circ Physiol. 2002;283:H2363–70.
43. Sutliff RL, Walp ER, El-Ali AM, Elkhatib S, Lomashvili KA, O'Neill WC. Effect of medial calcification on vascular function in uremia. Am J Physiol Ren Physiol. 2011;301:F78–83.
44. Boggy GJ, Woolf PJ. A mechanistic model of PCR for accurate quantification of quantitative PCR data. PLoS ONE. 2010;5:e12355.
45. Ritz C, Spiess AN. qpcR: an R package for sigmoidal model selection in quantitative real-time polymerase chain reaction analysis. Bioinformatics. 2008;24:1549–51.
46. Qiu H, Zhu Y, Sun Z, Trzeciakowski JP, Gansner M, Depre C, et al. Short communication: vascular smooth muscle cell stiffness as a mechanism for increased aortic stiffness with aging. Circ Res. 2010;107:615–9.
47. Castorena-Gonzalez JA, Staiculescu MC, Foote CA, Polo-Parada L, Martinez-Lemus LA. The obligatory role of the actin cytoskeleton on inward remodeling induced by dithiothreitol activation of endogenous transglutaminase in isolated arterioles. Am J Physiol Heart Circ Physiol. 2014;306:H485–95.

48. Castorena-Gonzalez JA, Staiculescu MC, Foote C, Martinez-Lemus LA. Mechanisms of the inward remodeling process in resistance vessels: is the actin cytoskeleton involved? Microcirculation. 2014;21:219–29.
49. McNulty M, Mahmud A, Spiers P, Feely J. Collagen type-I degradation is related to arterial stiffness in hypertensive and normotensive subjects. J Hum Hypertens. 2006;20:867–73.
50. Alajbegovic A, Holmberg J, Albinsson S. Molecular regulation of arterial aneurysms: role of actin dynamics and microRNAs in vascular smooth muscle. Front Physiol. 2017;8:569.
51. de Cavanagh EM, Ferder M, Inserra F, Ferder L. Angiotensin II, mitochondria, cytoskeletal, and extracellular matrix connections: an integrating viewpoint. Am J Physiol Heart Circ Physiol. 2009;296:H550–8.
52. Lassegue B, Sorescu D, Szocs K, Yin Q, Akers M, Zhang Y, et al. Novel gp91(phox) homologues in vascular smooth muscle cells: nox1 mediates angiotensin II-induced superoxide formation and redox-sensitive signaling pathways. Circ Res. 2001; 88:888–94.
53. Standley PR, Cammarata A, Nolan BP, Purgason CT, Stanley MA. Cyclic stretch induces vascular smooth muscle cell alignment via NO signaling. Am J Physiol Heart Circ Physiol. 2002;283: H1907–14.
54. Kanda K, Matsuda T. Behavior of arterial wall cells cultured on periodically stretched substrates. Cell Transplant. 1993;2: 475–84.
55. O'Connell MK, Murthy S, Phan S, Xu C, Buchanan J, Spilker R, et al. The three-dimensional micro- and nanostructure of the aortic medial lamellar unit measured using 3D confocal and electron microscopy imaging. Matrix Biol. 2008;27:171–81.
56. Wilson E, Vives F, Collins T, Ives HE. Strain-responsive regions in the platelet-derived growth factor-A gene promoter. Hypertension. 1998;31(1 Pt 2):170–5.
57. Iwasaki H, Eguchi S, Ueno H, Marumo F, Hirata Y. Mechanical stretch stimulates growth of vascular smooth muscle cells via epidermal growth factor receptor. Am J Physiol Heart Circ Physiol. 2000;278:H521–9.
58. Hu B, Song JT, Qu HY, Bi CL, Huang XZ, Liu XX, et al. Mechanical stretch suppresses microRNA-145 expression by activating extracellular signal-regulated kinase 1/2 and upregulating angiotensin-converting enzyme to alter vascular smooth muscle cell phenotype. PLoS ONE. 2014;9: e96338.
59. Rodriguez AI, Csanyi G, Ranayhossaini DJ, Feck DM, Blose KJ, Assatourian L, et al. MEF2B-Nox1 signaling is critical for stretch-induced phenotypic modulation of vascular smooth muscle cells. Arterioscler Thromb Vasc Biol. 2015;35:430–8.
60. Seo KW, Lee SJ, Kim YH, Bae JU, Park SY, Bae SS, et al. Mechanical stretch increases MMP-2 production in vascular smooth muscle cells via activation of PDGFR-beta/Akt signaling pathway. PLoS ONE. 2013;8:e70437.
61. Joki N, Kaname S, Hirakata M, Hori Y, Yamaguchi T, Fujita T, et al. Tyrosine-kinase dependent TGF-beta and extracellular matrix expression by mechanical stretch in vascular smooth muscle cells. Hypertens Res. 2000;23:91–9.
62. Abe K, Nakashima H, Ishida M, Miho N, Sawano M, Soe NN, et al. Angiotensin II-induced osteopontin expression in vascular smooth muscle cells involves Gq/11, Ras, ERK, Src and Ets-1. Hypertens Res. 2008;31:987–98.
63. Moran CS, Rush CM, Dougan T, Jose RJ, Biros E, Norman PE, et al. Modulation of kinin B2 receptor signaling controls aortic dilatation and rupture in the angiotensin II-infused apolipoprotein E-deficient mouse. Arterioscler Thromb Vasc Biol. 2016; 36:898–907.
64. Weisberg AD, Albornoz F, Griffin JP, Crandall DL, Elokdah H, Fogo AB, et al. Pharmacological inhibition and genetic deficiency of plasminogen activator inhibitor-1 attenuates angiotensin II/salt-induced aortic remodeling. Arterioscler Thromb Vasc Biol. 2005;25:365–71.
65. Bardy N, Merval R, Benessiano J, Samuel JL, Tedgui A. Pressure and angiotensin II synergistically induce aortic fibronectin expression in organ culture model of rabbit aorta. Evidence for a pressure-induced tissue renin-angiotensin system. Circ Res. 1996;79:70–8.